CANADIAN JOURNAL OF EXPLORATION GEOPHYSICS
VOL. 26, NOS. 1 & 2 (DECEMBER 1990), P. 33-46

SEAFLOOR SEISMIC VELOCITY: RESULTS FROM AN ANALYSIS OF THE WATER BOTTOM MULTIPLES RECORDED FROM THE ARCTIC ICE ISLAND EXPERIMENT

X. ZENG[1] AND R.F. MEREU[1]

ABSTRACT

The ice island experiment was a novel seismic reflection survey conducted on a floating ice sheet in the Arctic Ocean by the Geological Survey of Canada in 1985. The seismic data recorded from the experiment are dominated by water bottom multiples which show distinct reverberation patterns. On each of the raw data shot sections there is an amplitude cutoff line below which the amplitude of the multiples falls off sharply. An examination of the raw data shows that the cutoff line appears to be a straight line across the section and the slope of the line varies from shot to shot.

Synthetic data computed in the frequency domain using generalized ray theory with horizontally layered seismic models without and with an ice layer show that the amplitude cutoff line is due to an abrupt change of the *P-P* reflection coefficient at the water-seafloor interface with the angle of incidence. In the case that the seafloor *S*-velocity is greater than the water *P*-velocity, it is the seafloor *S*-velocity that determines the slope of the cutoff line. In the case that the seafloor *S*-velocity is smaller than the water *P*-velocity, it is the seafloor *P*-velocity that determines the slope. For both cases, the cutoff line is associated with the critical angle at the water-seafloor interface and the slope is proportional to the seafloor velocity. An analysis of the synthetic data and the real data from the ice island experiment shows that the velocity of seafloor sediments varies from 1.62 km/s to 2.18 km/s along the survey line.

INTRODUCTION

Water reverberation is often considered as an undesired noise which deteriorates the quality of marine seismic data. Backus (1959) studied the formation of the water reverberation patterns of marine seismic data and argued that some subsurface structural information is contained in these data even in their original forms. They are often characterized by an apparent ringing or dominant repetition interval, by an abnormal slow energy decay and by periodic multiples. The properties of the seafloor are very important parameters in the formation of the water reverberation patterns of these data. The large amplitude water bottom multiples which appear periodically at the critical angle in the seismic data from the Barents Sea, north of Norway, were used by Berge et al. (1986) to determine the seafloor velocity.

Seismic data recorded in the summer of 1985 from the Arctic ice island experiment are dominated by water bottom multiples. The processing and interpretation of the data are very difficult because of their low signal-to-noise ratio, (Cox, 1987; Hajnal and Overton, 1987; Cox et al., 1990). The multiples which plague the data are reflected at the water bottom in a wide range of angles of incidence and are characterized by their large amplitudes. They show very distinct reverberation patterns. One of the most prominent features is the amplitude cutoff line of the multiples. The amplitude of the multiples falls off sharply below this line on each of the shot sections of the raw data.

In this paper, a method similar to that of Berge et al. (1986) is investigated and applied to the Arctic ice island data sets. We show how the amplitude cutoff line is formed and how the variation of seafloor velocity can be inferred from the cutoff line by using synthetic data computed with horizontally layered models. The synthetic data are computed using generalized ray theory in the frequency domain where the effect of the complex reflection and transmission coefficient can be easily included. The free surface and geometrical spreading effects are also included in the modelling. The dominant frequencies of the source wavelets used are in the 22 to 25 Hz range. One essential purpose of the paper is to show how the ice layer affects the water reverberation patterns using a comparison of synthetic data from models without and with an ice layer.

EXPERIMENTAL SETUP AND RAW DATA

In 1983, an ice island, approximately 7 km by 3 km and 45 m thick, separated from the Arctic ice cap at the northern tip of Ellesmere Island and began to drift southward with the ocean currents (Figure 1a). In 1985, the Geological Survey of Canada installed a permanent seismic array on the moving ice island and conducted a seismic reflection survey to

Manuscript received by the Editor March 29, 1990; revised manuscript received August 10, 1990.
[1]Department of Geophysics, University of Western Ontario, London, Ontario N6A 5B7
We are grateful to Mr. A. Overton of the Geological Survey of Canada for making the Arctic ice island data available to us. This research was supported by the Natural Sciences and Engineering Research Council of Canada (NSERC) research grant A-1793.

study the structure of the sediments of the continental shelf under the Arctic Ocean floor. Further details on this experiment were presented by Cox (1987), Hajnal and Overton (1987) and Cox et al. (1990).

The seismic array used in the reflection experiment was a cross-arm array as shown in Figure 1b. The main line was about 3.53 km in length and had 107 stations with a station spacing of 33.33 m. The cross-arm line consisted of 12 stations. Each experiment on the ice island consisted of 13 shots. The source was located in the water at a depth of about 110 m from the top of the ice layer and consisted of 1 kg charges of 60 percent Geogel. All thirteen shots were fired 30 to 60 seconds apart with the set forming one shooting position. After the island had drifted for 1 km, the shots were fired again to form another shooting position. Altogether 87 shooting positions were covered and 975 shots were recorded during the summer of 1985.

Figures 2a to 2d show four shot sections of the raw data from the main line of the array. Shot 29 represents a typical shot where the water depth is deep, and shot 817 represents a typical shot where the water depth is shallow. Their water reverberation patterns are similar to those observed in the entire data sets. Shots 582 and 401 are two extreme examples from the experiment which show how the position of the cutoff line can vary. The large amplitude waves in the triangular area with an apparent velocity in the range of about 0.98 km/s to 1.48 km/s are the water bottom multiples. The amplitude of the multiples falls off sharply at some certain cutoff time for a given offset. The cutoff time varies with the offset. The line which links the location where the amplitude of the multiple falls off sharply is referred to as the amplitude cutoff line. The cutoff line appears to be approximately a straight line across the section as marked on each of the four sections. It seems that the multiples have gone through an on-and-off gate. All multiples above a certain threshold are passed through the gate and those below it are terminated.

Other main features of the raw data are: 1) initial large amplitude waves on large offset traces, 2) shingling waves on small offset traces, and 3) attenuation of the later phases on the large offset traces. The similarity of the wave patterns of the multiples for different shots of the raw data indicates that the multiples are coherent and are of a deterministic nature.

Although there is similarity in the major appearance, the variation in the slope of the amplitude cutoff line from shot to shot is significant. Figures 2c and 2d give a striking comparison of the slope of the cutoff line. The number of multiples which can be counted in Figure 2d is much greater than that in Figure 2c.

Theoretical Results

Introduction

The theory used to generate the synthetic data is similar to that of the generalized geometrical ray theory which decomposes the total wave field into the summation of infinite phases travelling along different raypaths. According to this theory, the complex amplitude of the synthetic seismogram at distance x can be computed in the frequency domain by

$$A(x,f) = W(f) \sum_{m=1}^{M} A_r A_f A_g A_q e^{-i2\pi f t_m}, \qquad (1)$$

where $W(f)$ is the complex spectrum of the source wavelet, M is the total number of individual waves considered, t_m is the traveltime, A_r is the total reflection and transmission coefficient, A_f is the free surface effect, A_g is the geometrical spreading effect, and A_q is a symbolic notation representing additional amplitude effects such as dissipation.

The reflection and transmission coefficients are obtained by solving the well-known Zoeppritz equations derived from a plane-wave ray theory. See, for example, McCamy et al. (1962) and Ben-Menahem and Singh (1981). They

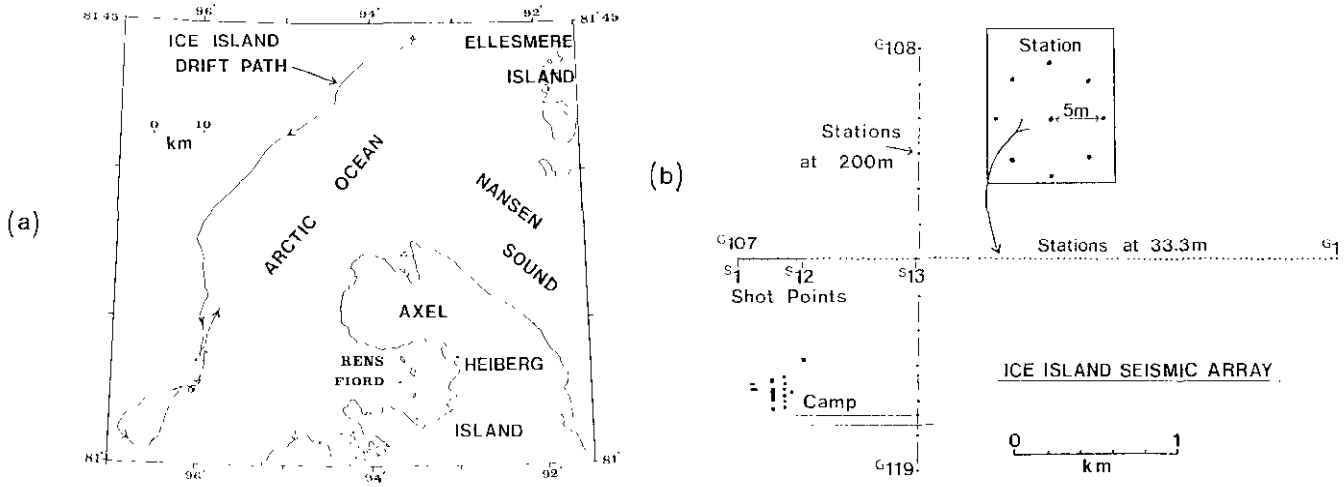

Fig. 1. (a) A map showing the drift path of the ice island during the summer of 1985 (after Cox, 1987). **(b)** Seismic array used to record the data in the ice island experiment. The main line has 107 stations. 13 shotpoints are located as shown with a source depth of about 110 m (after Cox, 1987).

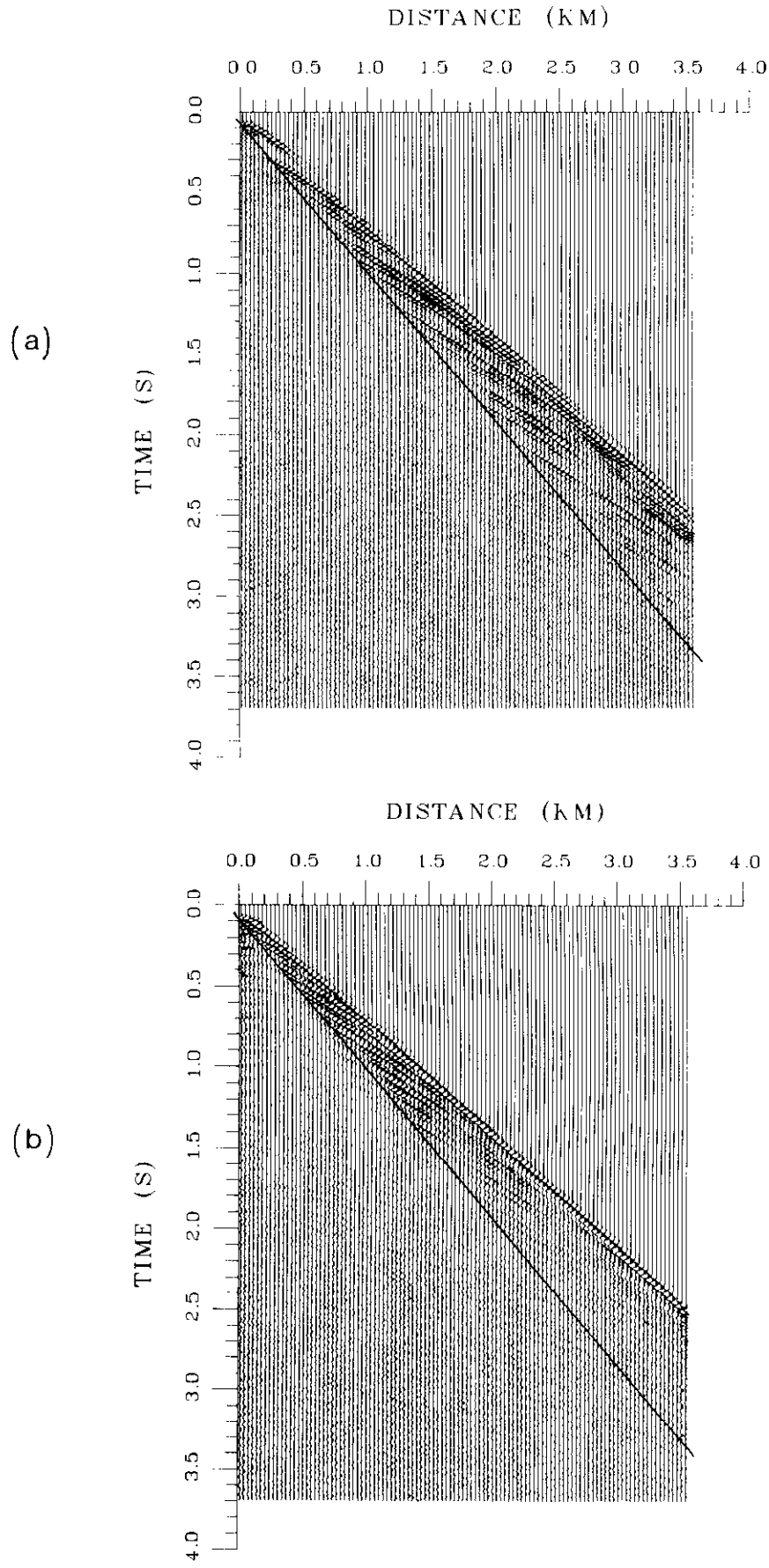

Fig. 2. (a) Display of shot section of the raw data of shot 29; **(b)** of shot 817.

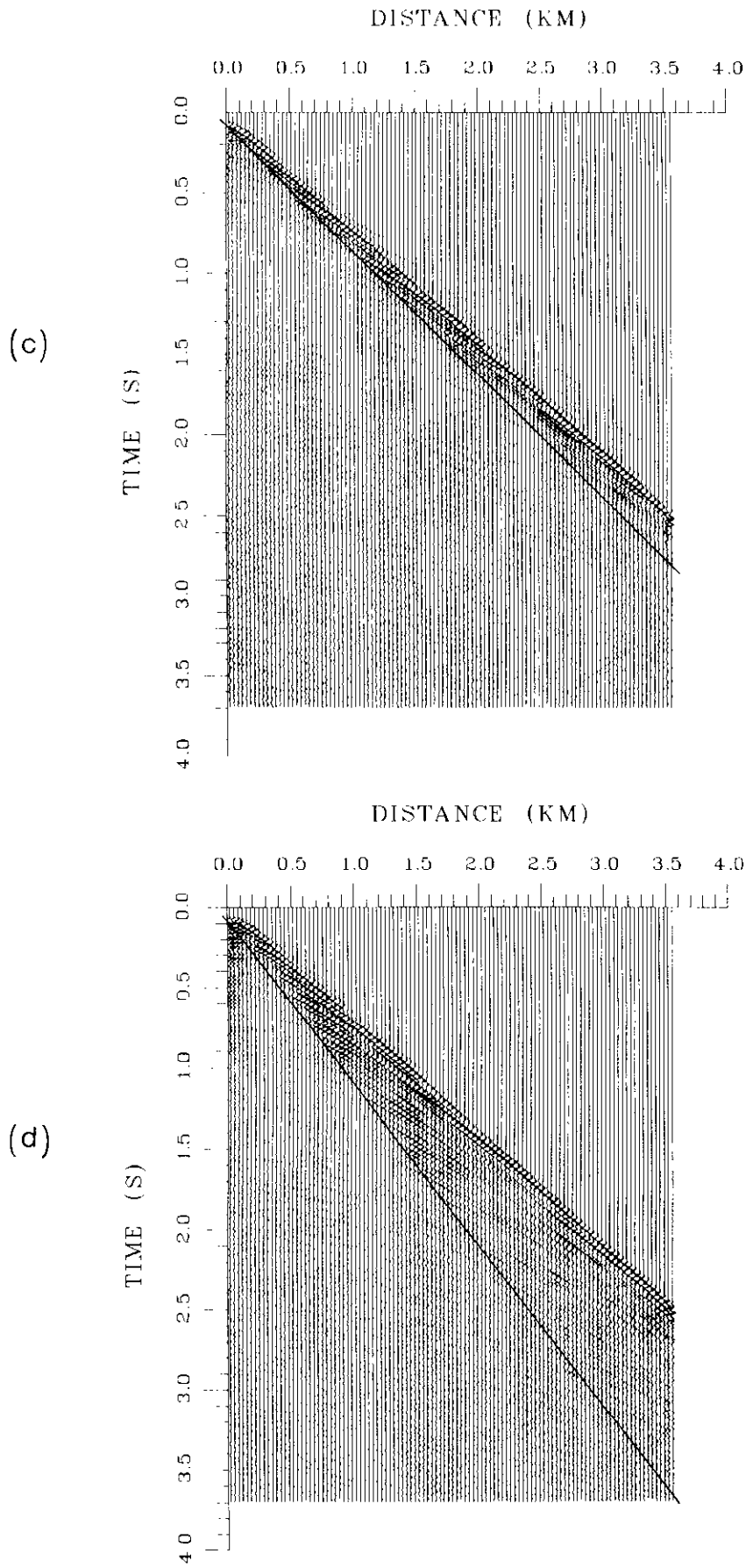

Fig. 2. (c) Display of shot section of the raw data of shot 582; **(d)** of shot 401.

are, in general, complex and are functions of the angle of incidence and the elastic properties of the media at both sides of the interface. The free surface effect is taken into account using plane-wave theory and, thus, A_f is also complex, while the geometrical spreading effect is computed in a manner similar to that given by Bullen (1963) and, thus, A_g is real. The effect of a complex coefficient can be easily incorporated in the frequency domain by a phase shift of the source wavelet. Taking an inverse Fourier transform of equation (1) provides a straightforward method for generating synthetic seismograms.

The seismic models used to compute synthetic seismograms in this paper are horizontal, layered models without and with an ice layer as shown in Figure 3. The no-ice model is a one-layered model and the ice model is a two-layered model. The main difference between the two models is that many more phases should be considered for the ice model. Each layer of the two models is specified by its *P*-velocity, *S*-velocity and density. For both models, the source is located in the water layer. The most important individual waves chosen for the ice model are the four groups of waves: 1) primary waves, 2) ice-water multiples, 3) ice multiples and 4) water multiples. The parameters of the two models used to generate synthetic data presented in this paper are listed in Table 1. In all cases, the parameters of the ice and water layers are kept constant. The 3.36 km/s value for the ice *P*-velocity is obtained from an analysis of the first-arrival least-squares lines of all the 975 shots from the ice island reflection experiment. The water *P*-velocity and the ice *S*-velocity are chosen to be 1.44 km/s and 1.48 km/s, respectively, to be consistent to the studies of Cox (1987) and Zeng (1989). The Poisson's ratio of a medium is derived from

$$\sigma = 0.5\,\frac{\alpha^2 - 2\beta^2}{\alpha^2 - \beta^2}$$

(Waters, 1981) when the *P*-velocity α and the *S*-velocity β are given.

A model is designated as a hard or soft model depending on whether the seafloor *S*-velocity is greater than the water *P*-velocity or not, respectively. For a model with a hard seafloor, there are two critical angles at the water-seafloor interface given by $i_{c1} = \sin^{-1}(\alpha_w/\alpha_s)$ and $i_{c2} = \sin^{-1}(\alpha_w/\beta_s)$;

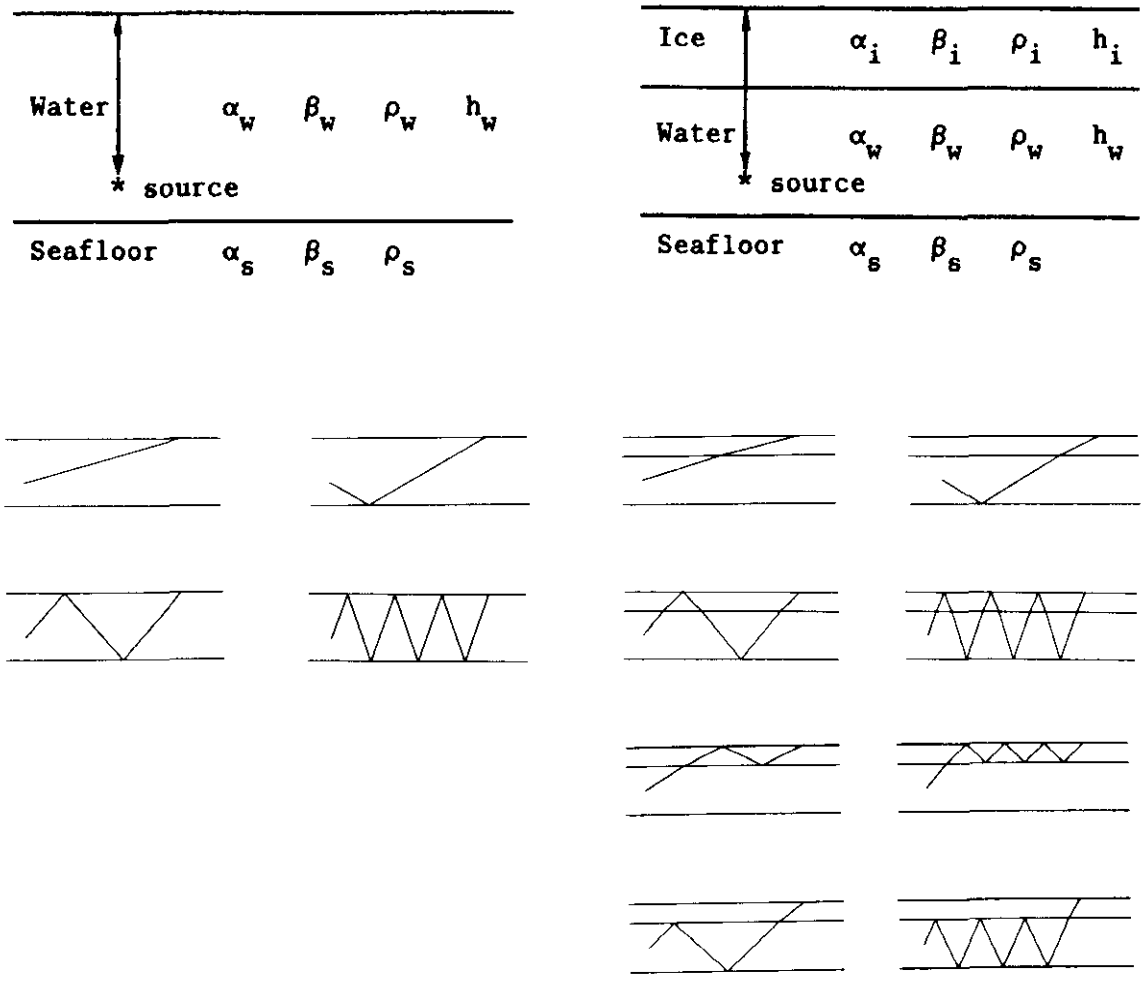

Fig. 3. The no-ice model and the ice model used to compute synthetic seismograms. Here α, β, ρ and *h* are the *P*-velocity, *S*-velocity, density and thickness of the layer. For both models, the source is located in the water layer. The raypaths shown for the ice model are the typical raypaths of the four groups of waves: 1) primary waves, 2) ice-water multiples, 3) ice multiples and 4) water multiples.

Case No.	Medium	*P*-velocity α(km/s)	*S*-velocity ß(km/s)	Poisson's ratio	Density ρ(g/cm3)	Thickness *h*(km)
1	Water	1.44	0.0	0.50	1.0	0.145
	Seafloor	4.0	2.0	0.33	2.4	
2	Water	1.44	0.0	0.50	1.0	0.145
	Seafloor	2.0	0.6	0.45	1.8	
3	Ice	3.36	1.48	0.38	0.9	0.045
	Water	1.44	0.0	0.50	1.0	0.100
	Seafloor	4.0	2.0	0.33	2.4	
4	Ice	3.36	1.48	0.38	0.9	0.045
	Water	1.44	0.0	0.50	1.0	0.100
	Seafloor	2.0	0.6	0.45	1.8	
5	Ice	3.36	1.48	0.38	0.9	0.045
	Water	1.44	0.0	0.50	1.0	0.100
	Seafloor	1.6	0.6	0.42	1.8	
6	Ice	3.36	1.48	0.38	0.9	0.045
	Water	1.44	0.0	0.50	1.0	0.100
	Seafloor	2.2	0.6	0.46	1.8	

Table 1. The parameters of the no-ice model and the ice model for 6 cases.

here α_w, α_s and β_s are the water *P*-, seafloor *P*- and seafloor *S*-velocities, respectively. The first critical angle corresponds to the angle of incidence in water when the transmitted *P*-wave in seafloor becomes evanescent, while the second critical angle occurs when the transmitted *S*-wave in seafloor becomes evanescent. For a model with a soft seafloor there is only one critical angle given by $i_{c1} = \sin^{-1}(\alpha_w/\alpha_s)$.

No-ice model

Although the no-ice model is an oversimplified model it was used in this study so that comparisons could be made with a model having an ice layer (see next section).

Figures 4a and 4b show how the *P-P* amplitude reflection coefficient at the water-seafloor interface is affected by variations of the seafloor *S*-velocity for a high-velocity seafloor case (α_s = 4.0 km/s) and for a low-velocity seafloor case (α_s = 2.0 km/s), respectively. It is clear that the seafloor *S*-velocity is very important when the angle of incidence is larger than the first critical angle for both cases.

The reflection coefficients at the water-seafloor interface were used to generate synthetic sections for a high-velocity seafloor model with a hard seafloor and for a low-velocity seafloor model with a soft seafloor. Typical reflection coefficient curves are shown in Figure 5a. The abrupt change of the reflection coefficient at about 46 degrees is due to the second critical angle for the high-velocity seafloor model with a hard seafloor and to the first critical angle for the low-velocity seafloor model with a soft seafloor. The total reflection coefficients for different multiples ranging from 1 to 11 for the model with a hard seafloor (case 1) are shown in Figure 5b. They are obtained by multiplication of the corresponding reflection coefficient at the water-seafloor interface shown in Figure 5a. These curves illustrate a possible cause of the cutoff line. Multiples reflected at the water bottom with an angle of incidence greater than the second critical angle are of large amplitude, and those

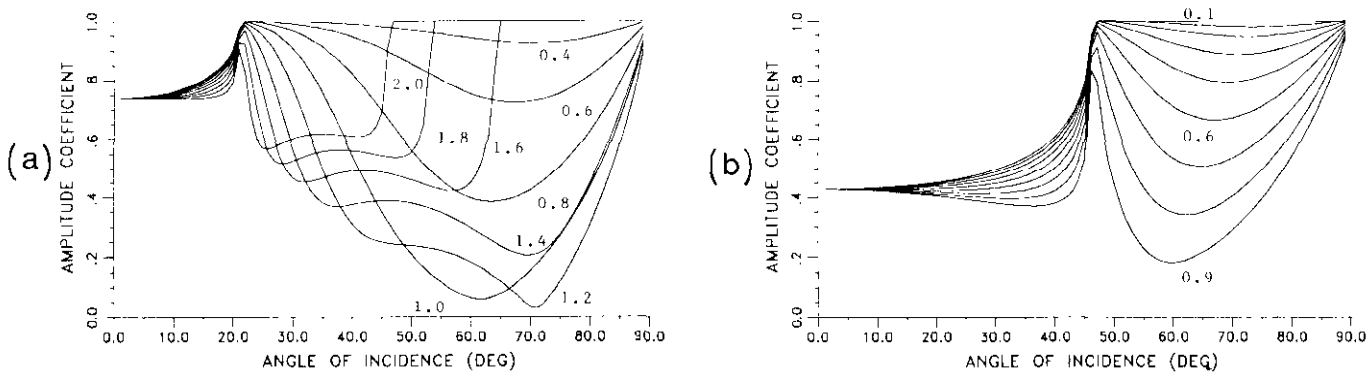

Fig. 4. (a) *P-P* reflection coefficient at the water-seafloor interface for different seafloor *S*-velocities for the high-velocity seafloor case. α_w = 1.44 km/s, β_w = 0, ρ_w = 1.0 g/cm^3, α_s = 4.0 km/s, ρ_s = 2.4 g/cm^3 and β_s = 0.4–2.0 km/s. The numbers represent β_s in km/s and the increment in β_s is 0.2 km/s. **(b)** *P-P* reflection coefficient at the water-seafloor interface for different seafloor *S*-velocities for the low-velocity seafloor case. α_w = 1.44 km/s, β_w = 0, ρ_w = 1.0 g/cm^3, α_s = 2.0 km/s, ρ_s = 1.8 g/cm^3 and β_s = 0.1–1.0 km/s. The numbers represent β_s in km/s and the increment in β_s is 0.1 km/s.

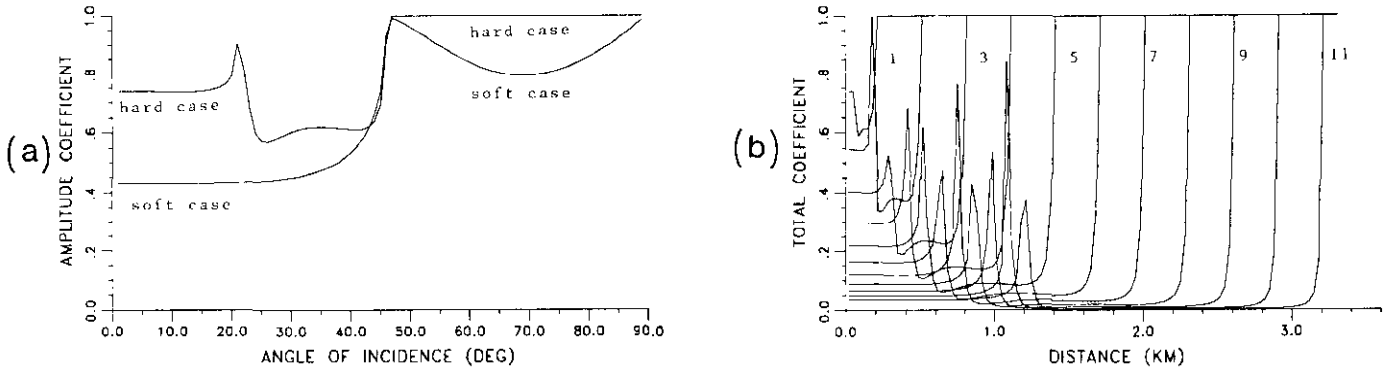

Fig. 5. (a) A comparison of the reflection coefficients at water-seafloor interface for a model with a hard seafloor and a model with a soft seafloor. The abrupt change of the reflection coefficient is due to the second critical angle for the hard seafloor case and due to the first critical angle for the soft seafloor case. Parameters are given in cases 1 and 2 in Table 1. **(b)** Total coefficients for downgoing multiples 1 to 11 for a no-ice model with a hard seafloor (case 1: α_s = 4.0 km/s, β_s = 2.0 km/s, σ_s = 0.33).

reflected with an angle of incidence smaller than the second critical angle are relatively very weak. It is apparent that the low-velocity seafloor model with a soft seafloor should have the same on-and-off mechanism which would produce an amplitude cutoff line on a shot section.

For a no-ice model, the traveltime and the offset for a particular multiple m are given by $t(m) = Z_w(m)/(\alpha_w \cos i_w)$ and $x(m) = Z_w(m)\tan i_w$, respectively. Here $Z_w(m)$ is the total vertical distance travelled by the multiple in the water layer, α_w is the water P-velocity and i_w is the angle of incidence in the water layer. The traveltime and the offset are related by

$$\frac{x(m)}{t(m)} = \alpha_w \sin i_w . \qquad (2)$$

It is interesting to note that the traveltime-offset relation does not depend on the rank of the multiple. Equation (2) simply indicates that all of the multiples with a given angle of incidence will arrive on a straight line on a shot section. For those multiples incident with a critical angle $i_c = \sin^{-1}(\alpha_w/v_s)$, the slope is given by

$$t_c/x_c = v_s/(\alpha^2_w), \qquad (3)$$

where x_c and t_c are the corresponding critical distance and critical time and v_s is the seafloor velocity. The slope of the cutoff line is proportional to the seafloor velocity, v_s, and does not depend on the water depth.

The synthetic section for a no-ice model with a hard seafloor (case 1: α_s = 4.0 km/s, β_s = 2.09 km/s, σ_s = 0.33) is shown in Figure 6. Multiples reflected with an angle of incidence close to the first critical angle or greater than the second critical angle show up as large amplitude waves. The amplitude cutoff line in the section is attributed to the steep decrease of the reflection coefficient at the second critical angle. The waves below the line do not show up because they are weak in comparison with the supercritically reflected earlier multiples in the same trace. This is due to their small total reflection coefficients. The slope of the cutoff line is in agreement with that given by equation (3). The synthetic section for a no-ice model with a soft seafloor (case 2: α_s = 2.0 km/s, β_s = 0.6 km/s, σ_s = 0.45) is shown in Figure 7. The slope of the cutoff line is about the same as that in Figure 6 since the abrupt change of the reflection coefficient at the water-seafloor interface occurs at the same angle of incidence for both cases. The seafloor S-velocity in the hard seafloor case is equal to the seafloor P-velocity in the soft seafloor case. The multiples which are associated with the first critical angle in Figure 6 do not show up in Figure 7 because the reflection coefficient is small at about 21 degrees for the soft seafloor case.

Ice model

It is more realistic to include the ice layer in computing the synthetic seismograms. Since the ice layer is a solid layer, there are both P- and S-waves in it. In this paper only the S-waves are considered in the ice layer since the large amplitude water bottom multiples observed in the real data transmit through the ice layer mainly as S-waves. Figure 8a shows how the energy is partitioned among the reflected P-, transmitted P- and transmitted S-waves when a P-wave is incident from the water layer at the water-ice interface. It is clear that most of the P-wave energy incident from water will convert to S-wave energy in ice since the P-S transmission coefficient is very large in the majority of range of angle of incidence (from 25 degrees to 65 degrees). Figure 8b shows how the P-S energy or the two-way amplitude transmission coefficient at the water ice interface varies with the S-velocity. Since the ice S-velocity is close to the water P-velocity, the P-S raypaths are only slightly bent at the water-ice interface. This would suggest that multiples made up of P-S raypaths for the ice model will probably have similar characteristics to the multiples observed for models without an ice layer.

For an ice model, the traveltime-offset formula contains terms of the ratio of the velocities as well as the ratio of the thicknesses of the ice and water layers. If the water P-velocity is equal to the ice S-velocity, this formula reduces to equation (3). Since the ice S-velocity is very close to the water P-velocity, equation (3) still holds approximately for

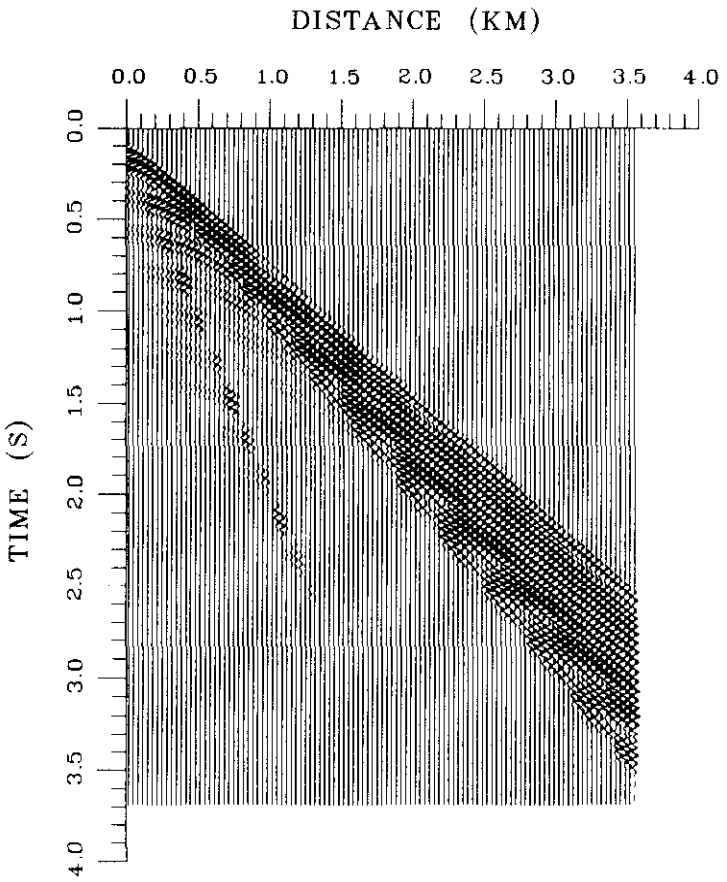

Fig. 6. Synthetic section for a no-ice model with a hard seafloor (case 1: $\alpha_s = 4.0$ km/s, $\beta_s = 2.0$ km/s, $\sigma_s = 0.33$).

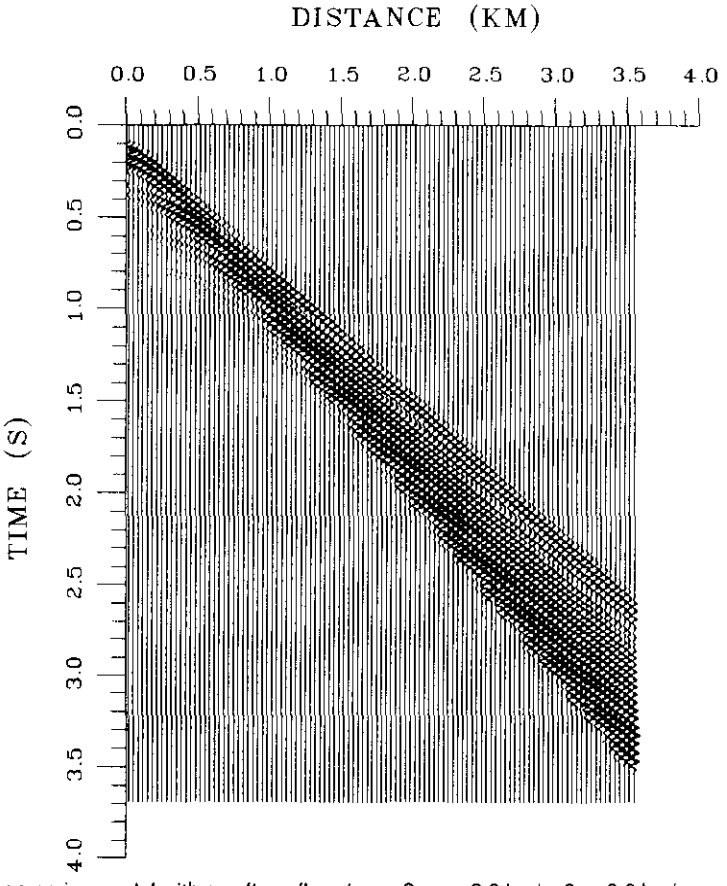

Fig. 7. Synthetic section for a no-ice model with a soft seafloor (case 2: $\alpha_s = 2.0$ km/s, $\beta_s = 0.6$ km/s, $\sigma_s = 0.45$).

the slope of the cutoff line for the ice model. A more detailed discussion of this analysis is given by Zeng (1989).

The synthetic sections for an ice model with a hard seafloor (case 3: α_s = 4.0 km/s, β_s = 2.0 km/s, σ_s = 0.33) and with a soft seafloor (case 4: α_s = 2.0 km/s, β_s = 0.6 km/s, σ_s = 0.45) are shown in Figures 9 and 10, respectively. The two synthetic sections are quite complicated due to the overlapping of various phases. In Figure 9, ice multiples and water multiples are seen in the earlier part of the multiple trains, while ice-water multiples dominate the later part. The weak zone between the two parts is due to the fact that the earlier ice-water multiples are weak and later ice multiples and water multiples are weak. Although the synthetic sections for the no-ice model and the ice model (compare Figures 6 and 7 with Figures 9 and 10) differ in detail, the cutoff lines are very clear for both models and the slopes of the cutoff lines are about the same due to the same value of the seafloor velocity used. This implies that the amplitude cutoff line is effectively due to the properties of the seafloor and the existence of the ice layer does not affect the slope of the cutoff line significantly.

Since the *P-P* reflection coefficient at the water-seafloor interface is very sensitive to the variation of the seafloor velocity, the synthetic section is also very sensitive to the variation of the seafloor velocity. Figures 11a and 11b show two synthetic sections for the ice model with soft seafloors α_s = 1.6 km/s and α_s = 2.2 km/s (cases 5 and 6), respectively. The only difference for cases 4, 5 and 6 is the seafloor *P*-velocity. A comparison of the corresponding synthetic sections in Figures 10, 11a and 11b shows that the variation of seafloor velocity changes the slope of the cutoff line in the way as specified by equation (3). Synthetic sections also demonstrate that this is true for the ice model with a hard seafloor. The slope of the cutoff line depends only on the seafloor velocity or on the critical angle i_c for a given water *P*-velocity. Figure 11c shows where the cutoff line should appear on a shot section for α_w = 1.44 km/s. Since a smaller critical angle corresponds to a larger seafloor velocity for a given water velocity and only those multiples which are reflected at an angle greater than the critical angle can survive, it is clear that the slope of the cutoff line is directly proportional to the seafloor velocity.

Results

An examination of 74 shots of the raw data from shotpoint 1 of the ice island experiment shows that the cutoff line on each of the shot sections does appear to be a straight line and the slope of the line varies from shot to shot. In general, the cutoff time is very sharp for small offset traces, and it becomes vague for large offset traces due to the attenuation of the later phases of the multiple trains. The location of the cutoff line was determined by eye according to the wave patterns on the whole section. The slopes measured for the 74 shots are listed in the second column in Table 2. The maximum uncertainty in the slope determined in this manner is about ±0.02 s/km. These slopes are converted to the seafloor velocities using equation (3) with α_w = 1.44 km/s and are listed in the third column. The uncertainty in these velocities is about ±0.04 km/s. These shots are located along the drift path of the ice island as shown in Figure 12a and the seafloor velocity profile obtained is plotted in Figure 12b. The velocity profile exhibits two velocity highs. The velocity high for shots 300 to 500 is actually compatible with the velocity high for shots 800 to 900 since the drift path is looped around to cover the same area. The velocity is slightly higher in the east side of the drift path and varies from 1.62 km/s for shot 582 to 2.18 km/s for shot 401.

Discussion and Conclusions

Although there is ambiguity in the seafloor model, we are quite confident in the validity of the mechanism of the cutoff line and its relationship to the seafloor velocity. If the seafloor sediments are hard, the cutoff line is due to the

Shot No.	Slope (s/km)	Velocity (km/s)	Shot No.	Slope (s/km)	Velocity (km/s)
2	0.87	1.81	505	0.94	1.94
15	0.93	1.93	516	0.90	1.87
29	0.93	1.93	526	0.82	1.71
43	0.93	1.93	549	0.91	1.89
56	0.87	1.81	560	0.86	1.78
70	0.86	1.78	571	0.90	1.87
83	0.92	1.90	582	0.78	1.62
96	0.88	1.82	603	0.81	1.68
111	0.94	1.94	614	0.85	1.75
123	0.89	1.84	625	0.87	1.81
139	0.86	1.78	636	0.87	1.81
166	0.86	1.78	648	0.86	1.79
182	0.86	1.78	659	0.84	1.74
196	0.85	1.76	670	0.82	1.71
209	0.85	1.76	681	0.83	1.73
222	0.85	1.76	692	0.83	1.73
235	0.87	1.81	703	0.86	1.78
249	0.84	1.74	715	0.85	1.76
261	0.86	1.78	726	0.83	1.73
276	0.85	1.76	737	0.82	1.71
289	0.79	1.64	748	0.84	1.74
304	0.82	1.69	759	0.83	1.73
317	0.80	1.66	770	0.87	1.81
329	0.81	1.68	795	0.81	1.67
342	0.87	1.81	806	0.95	1.97
354	0.93	1.93	817	0.93	1.93
365	1.03	2.13	828	0.96	1.99
377	1.00	2.07	839	0.95	1.97
389	1.01	2.09	851	0.96	1.99
401	1.05	2.18	873	0.90	1.86
415	1.01	2.09	884	0.82	1.71
426	0.94	1.95	895	0.84	1.74
436	1.04	2.16	906	0.87	1.80
447	1.01	2.09	917	0.86	1.78
460	1.04	2.16	928	0.86	1.79
480	1.00	2.07	939	0.95	1.96
497	0.91	1.89	950	0.96	1.99

Table 2. Slopes of the amplitude cutoff lines and seafloor velocities *for 74 shots from the ice island experiment. The maximum uncertainties* are 0.02 s/km in the slope and 0.04 km/s in the seafloor velocity.

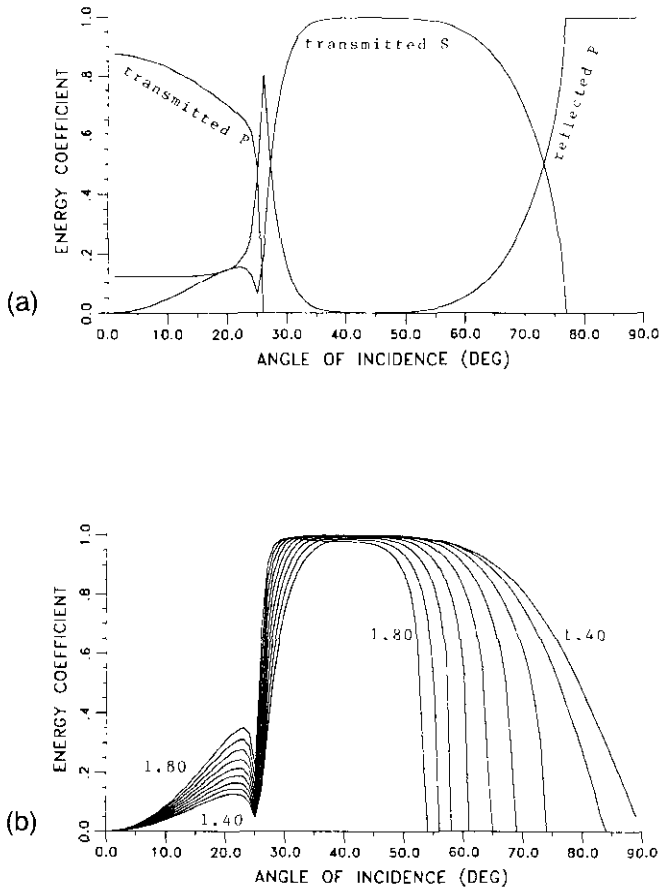

Fig. 8. **(a)** Energy coefficients for a *P*-wave incident at the water-ice interface. α_w = 1.44 km/s, β_w = 0, ρ_w = 1.0 g/cm^3, α_i = 3.36 km/s, β_i = 1.48 km/s and ρ_i = 0.9 g/cm^3. **(b)** *P-S* energy transmission coefficients at the water-ice interface for a *P* incident wave for different ice *S*-velocities. α_w = 1.44 km/s, β_w = 0, ρ_w = 1.0 g/cm^3, α_i = 3.36 km/s and ρ_i = 0.9 g/cm^3 and β_i = 1.40 -1.80 km/s. The numbers represent β_i in km/s and the increment in β_s is 0.05 km/s.

second critical angle and the velocity profile in Figure 12b will represent a seafloor *S*-velocity profile. If the seafloor sediments are soft, the cutoff line is due to the first critical angle and the velocity profile in Figure 12b will represent a seafloor *P*-velocity profile.

Attempts to compare our velocity values in Figure 12b to the velocity values obtained from a first-arrival refraction analysis of the raw data were not successful. The most significant observation of the first-arrival data was the fact that the traveltime curve for the ice layer turned out to be very dominant and was present with the same slope and intercept on almost all the data sets. The analysis of all the 975 shots showed that the ice *P*-velocity was in the 3.27 to 3.45 km/s range with an average value of 3.36 km/s. The intercept time for the ice traveltime line was consistent with an ice thickness of approximately 40 to 45 m. Figures 13a and 13b show two typical first-arrival data sets. Figure 13a has only one traveltime line. This is the "ice" layer line. The figure shows that this line can easily be the first arrival for the whole section. All refraction energy from the sedimentary layers below the water comes in as later arrivals. Thus, it is impossible to determine the seafloor velocity from a first-arrival analysis of this type of data. This occurs when the ocean water is deeper than a critical depth of 250 to 300 m. For shallower depths, the pattern of the first arrivals is different, as is illustrated in Figure 13b. Here, the traveltime branches from both deeper high-velocity sediments (4.0 km/s and 5.3 km/s) are observed at the far end of the line. No sediment whose velocity is less than that of the ice *P*-velocity will produce a first-arrival refraction traveltime branch. Since there are considerable shallow structural and topographic variations in the area, the velocity profile we obtained would possibly represent the velocity at the very top of the seafloor sediments.

Asudeh et al. (1988) carried out a long-range refraction survey for a number of lines in the same area in 1985. Their data showed that the *P*-velocities of the seafloor sediments varied from 2.2 km/s to 3.7 km/s and increased through a succession of layers to 6.0 km/s. The total thickness of the sediments was found to be up to 5 km. Another possible interpretation of the seafloor is that there is an unconsolidated soft thin layer overlying the hard sedimentary rock layers as mentioned by Hobson (1989).

This method of using the cutoff line appears to be particularly useful and effective for the determination of the seafloor velocity in a shallow area where angles of incidence for different multiples can easily go beyond the critical angle at the water-seafloor interface. This method is applicable in both cases without and with an ice layer.

References

Asudeh, I., Forsyth, D.A., Stephenson, R., Embry, A., Jackson, H.R. and White, D., 1988, Crustal structure of the Canadian polar margin: results of the 1985 seismic refraction survey: Geol. Surv. Can., contribution 44687.

Backus, M.M., 1959, Water reverberations – their nature and elimination: Geophysics **24**, 233-261.

Ben-Menahem A. and Singh, S.J., 1981, Seismic waves and sources: Springer-Verlag New York, Inc.

Berge, A.M., Drivenes, G., Kanestrøm, R. and Beskow, B., 1986, Acoustic modeling of the seafloor: Geophys. Prosp. **34**, 11-29.

Bullen, K.E., 1963, An introduction to the theory of seismology: Cambridge Univ. Press, 125-127.

Cox, T.P., 1987, Evaluation of various processing techniques applied to seismic data recorded from an ice island in the Arctic ocean, Canada: M.Sc. thesis, Univ. of Western Ontario.

_____, Overton, A. and Mereu, R.F., 1990, Seismic reflection results from an ice island over the Arctic continental shelf: Tectonophys. **93**, 193-210.

Hajnal, Z. and Overton, A., 1987, Reflection experiment on a floating ice platform: Geophys. J.Roy Astr. Soc. **89**, 201-208.

Hobson, G., 1989, Ice Island field station – new features of Canadian polar margin: EOS **70.**

McCamy, K., Meyer, R.P. and Smith, T.J., 1962, Generally applicable solutions of Zoeppritz amplitude equations: Bull. Seis. Soc. Am. **52**, 923-955.

Waters, K.H., 1981, Reflection seismology – a tool for energy resource exploration: A Wiley-Interscience publication, 22.

Zeng, X., 1989, Amplitude modeling of the water bottom multiple waves of the seismic data recorded in the Arctic ice island experiment: M.Sc. thesis, Univ. of Western Ontario.

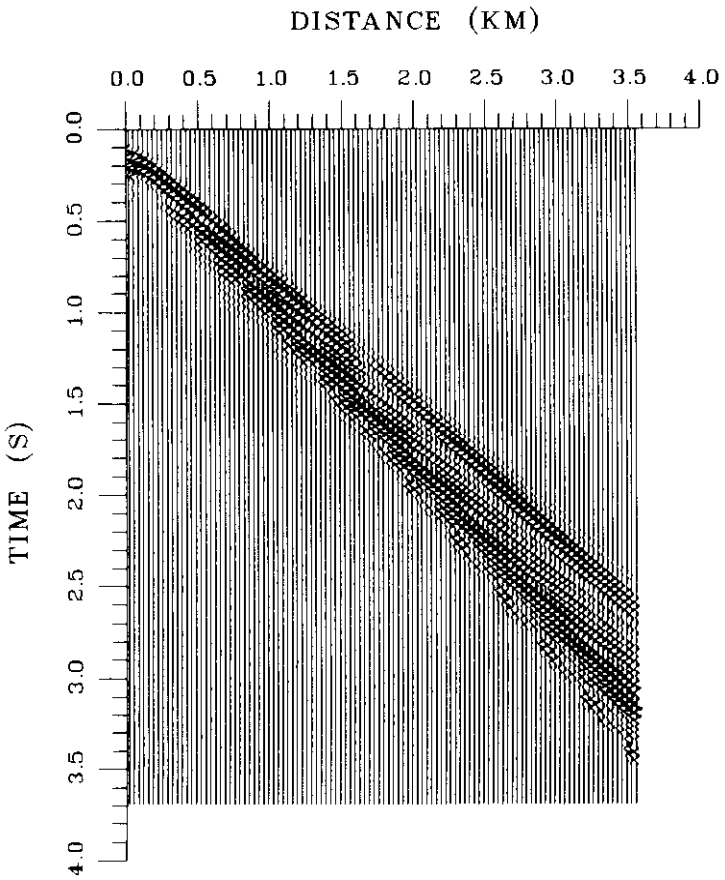

Fig. 9. Synthetic section for an ice model with a hard seafloor (case 3: $\alpha_s = 4.0$ km/s, $\beta_s = 2.0$ km/s, $\sigma_s = 0.33$).

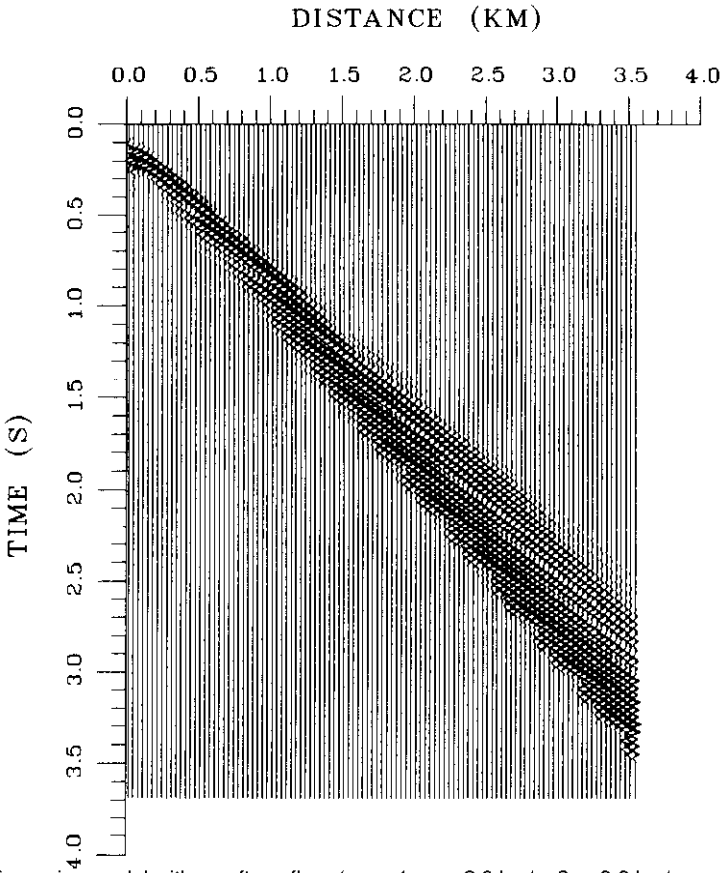

Fig. 10. Synthetic section for an ice model with a soft seafloor (case 4: $\alpha_s = 2.0$ km/s, $\beta_s = 0.6$ km/s, $\sigma_s = 0.45$).

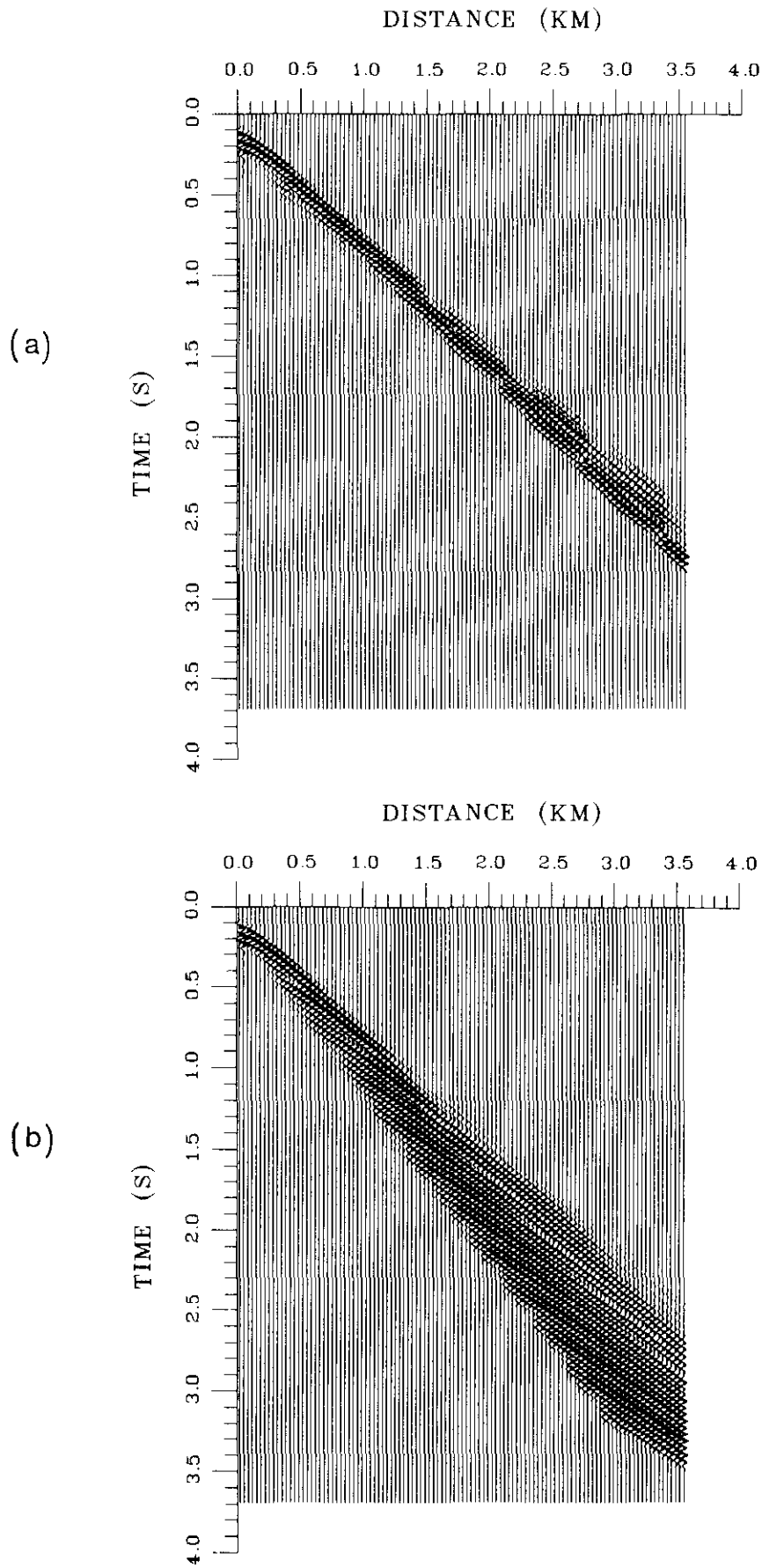

Fig. 11. **(a)** Synthetic section for an ice model with a soft seafloor (case 5: α_s = 1.6 km/s, β_s = 0.6 km/s, σ_s = 0.42); **(b)** (case 6: α_s = 2.2 km/s, β_s = 0.6 km/s, σ_s = 0.46).

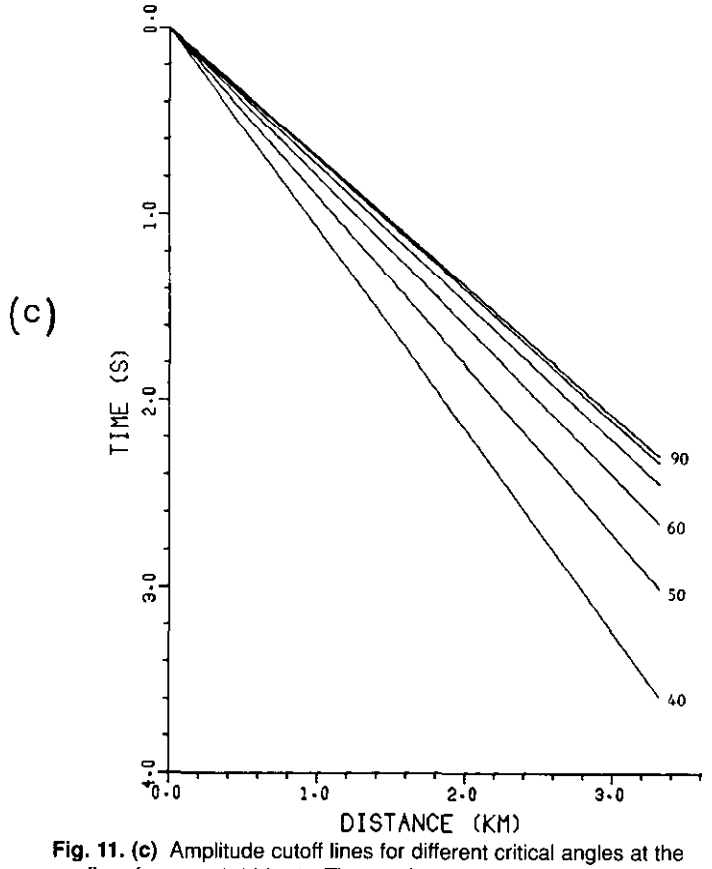

Fig. 11. (c) Amplitude cutoff lines for different critical angles at the seafloor for α_w = 1.44 km/s. The numbers are the critical angles in degrees.

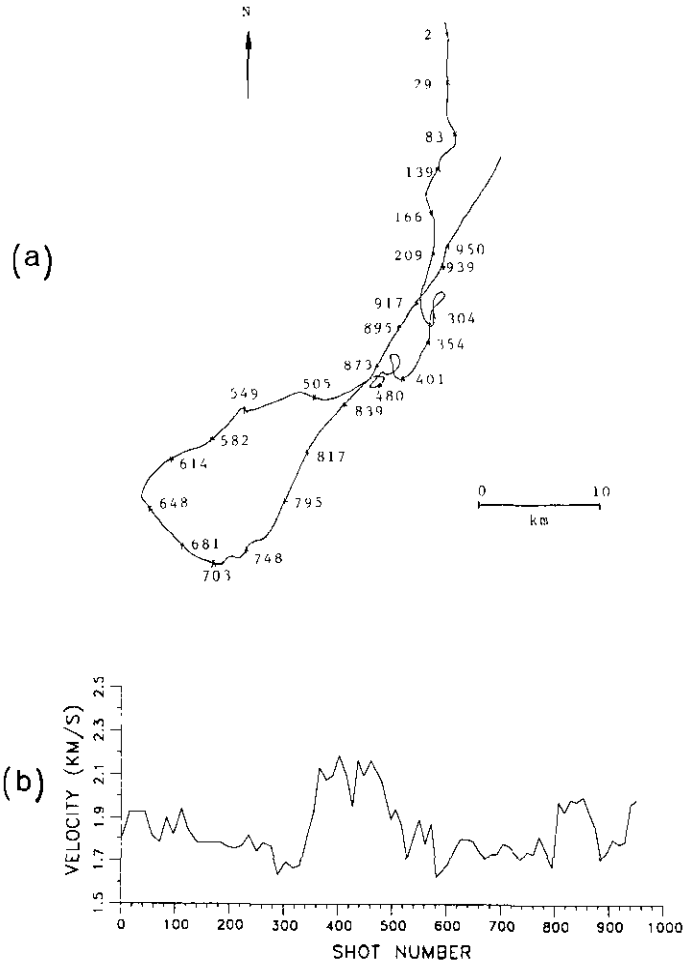

Fig. 12. (a) The locations of different shots along the drift path of the ice island. The numbers are the shot numbers. **(b)** Seafloor velocity profile along the drift path shown in Figure 12(a).

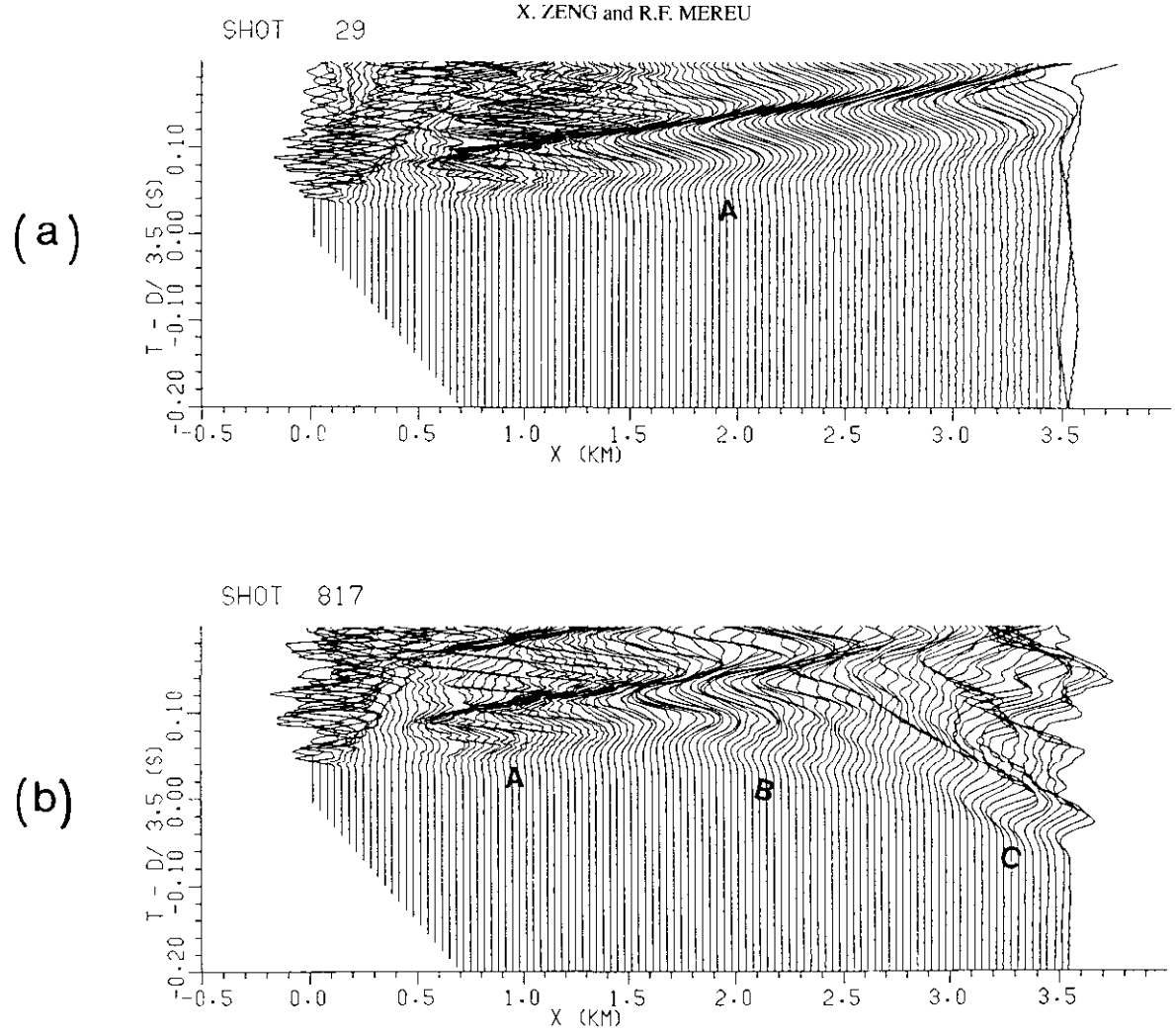

Fig. 13. (a) First-arrival data for shot 29. The main traveltime branch (*A*) is a *P*-wave branch from the ice layer with a velocity of 3.36 km/s. **(b)** First-arrival data for shot 817. There is an ice branch (*A*) with a velocity of 3.36 km/s and two sedimentary branches (*B*) and (*C*) with velocities 4.0 km/s and 5.3 km/s.